Acta Crystallographica Section F
Structural Biology and Crystallization Communications
ISSN 1744-3091

Juliana Barbosa Coitinho, Débora Maria Abrantes Costa, Samuel Leite Guimarães, Alfredo Miranda de Góes and Ronaldo Alves Pinto Nagem*

Departamento de Bioquímica e Imunologia, Instituto de Ciências Biológicas, Universidade Federal de Minas Gerais, Avenida Antônio Carlos 6627, 31270-901 Belo Horizonte-MG, Brazil

Correspondence e-mail: nagem@icb.ufmg.br

Received 20 September 2011
Accepted 23 November 2011

Expression, purification and preliminary crystallographic studies of NahF, a salicylaldehyde dehydrogenase from *Pseudomonas putida* G7 involved in naphthalene degradation

Pseudomonas putida G7 is one of the most studied naphthalene-degrading species. The *nah* operon in *P. putida*, which is present on the 83 kb metabolic plasmid NAH7, codes for enzymes involved in the conversion of naphthalene to salicylate. The enzyme NahF (salicylaldehyde dehydrogenase) catalyzes the last reaction in this pathway. The *nahF* gene was subcloned into the pET28a(TEV) vector and the recombinant protein was overexpressed in *Escherichia coli* Arctic Express at 285 K. The soluble protein was purified by affinity chromatography followed by gel filtration. Crystals of recombinant NahF (6×His-NahF) were obtained at 291 K and diffracted to 2.42 Å resolution. They belonged to the hexagonal space group $P6_422$, with unit-cell parameters $a = b = 169.47$, $c = 157.94$ Å. The asymmetric unit contained a monomer and a crystallographic twofold axis generated the dimeric biological unit.

1. Introduction

Polycyclic aromatic hydrocarbons (PAHs) are a group of aromatic hydrocarbons composed of two or more fused rings and include naphthalene, anthracene, phenanthrene, pyrene and benzo[*a*]pyrene amongst others (Haritash & Kaushik, 2009). PAHs from natural and anthropogenic sources are widely distributed in the environment (Kanaly & Harayama, 2000). These compounds have a high stability and a low solubility in water, which contribute to their persistence in the environment (Samanta *et al.*, 2002; Haritash & Kaushik, 2009).

Exposure to naphthalene has been associated with several toxic manifestations in humans and laboratory animals, with the lens of the eye and the lungs being most sensitive (Stohs *et al.*, 2002). Additionally, this compound has been reclassified as a possible human carcinogen by the US Environmental Protection Agency (EPA, 2004) and the International Agency for Research on Cancer (IARC, 2002). It has recently been suggested that naphthalene undergoes metabolic activation to 1,2-naphthoquinone, which reacts with DNA, leading to the formation of apurinic sites on DNA and depurinating DNA adducts (Saeed *et al.*, 2009).

Moreover, a number of studies have attested to the carcinogenic and mutagenic properties of more complex PAHs (Park *et al.*, 2006; Spink *et al.*, 2008; Topinka *et al.*, 2008), suggesting the need for further work on the elimination of these compounds from the environment. Bioremediation might be a potential strategy to achieve this purpose (Kanaly & Harayama, 2000). Briefly, this strategy involves the use of microorganisms or enzymes capable of metabolizing toxic compounds, such as PAHs, into substances that have little or no toxicity (Holliger *et al.*, 1997).

Bacterial strains such as those from the genera *Mycobacterium*, *Corynebacterium*, *Flavobacterium*, *Rhodococcus*, *Bacillus* and particularly *Pseudomonas* that are able to degrade aromatic hydrocarbons have been widely described (Cerniglia, 1984; Annweiler *et al.*, 2000; Kanaly & Harayama, 2000; Arun *et al.*, 2008). Species of the genus *Pseudomonas* are metabolically versatile and use a large number of organic compounds as carbon sources, including aromatic hydrocarbons such as naphthalene (Rosselló-Mora *et al.*, 1994).

There are several reports in the literature of complete nucleotide sequences coding for enzymes involved in naphthalene-degradation pathways in bacteria. The chromosome of *P. stutzeri* AN10 and

plasmids from *P. putida* ND6, *P. putida* NCIB 9816-4 and *P. putida* G7 contain the genes of this pathway (Bosch *et al.*, 1999; Dennis & Zylstra, 2004; Li *et al.*, 2004).

The Gram-negative bacterium *P. putida* G7 is among the best studied naphthalene-degrading species. The genes associated with naphthalene metabolism are localized on NAH7, an 83 kilobase plasmid (Yen & Gunsalus, 1982). Other species also have naphthalene catabolic plasmids that are quite similar to NAH7: pWW60 derivatives from *P. putida* strain NCIB 9816 (Yang *et al.*, 1994), pDTG1 from *P. putida* strain NCIB 9816-4 (Dennis & Zylstra, 2004) and pKA1 from *P. fluorescens* strain 5R (Habe & Omori, 2003).

In *P. putida* G7 the naphthalene-oxidation genes are organized into two operons under salicylate control. The first operon, which is associated with the upper naphthalene-degradation pathway, includes the genes *nahAaAbAcAdBCDEF*, which code for the conversion of naphthalene to salicylate, while the second operon includes the genes *nahGTHINLOMKJ* coding for the lower pathway that includes the oxidation of salicylate *via* the catechol *meta*-cleavage pathway (Yen & Gunsalus, 1985).

The first step in naphthalene catabolism is the incorporation of molecular oxygen into the aromatic nucleus of naphthalene to produce *cis*-1,2-dihydroxy-1,2-dihydronaphthalene (Fig. 1). This reaction is catalyzed by the naphthalene dioxygenase (NDO) complex, which is composed of four proteins: ferredoxin reductase (NahAa), ferredoxin (NahAb) and two iron–sulfur proteins (NahAc and NahAd). The four subsequent reactions are catalyzed by *cis*-naphthalene dihydrodiol dehydrogenase (NahB), 1,2-dihydroxynaphthalene dioxygenase (NahC), 2-hydroxy-2*H*-chromene-2-carboxylate isomerase (NahD) and *trans-o*-hydroxybenzylidenepyruvic hydratase-aldolase (NahE), resulting in the formation of salicylaldehyde (Davies & Evans, 1964).

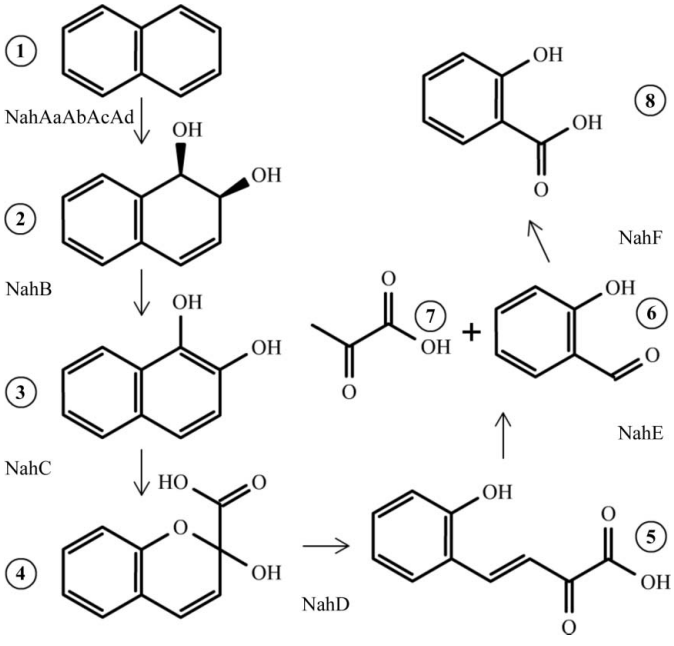

Figure 1
Naphthalene-degradation upper pathway. The upper pathway is composed of NahAaAbAcAd (naphthalene dioxygenase complex; NDO), *cis*-naphthalene dihydrodiol dehydrogenase (NahB), 1,2-dihydroxynaphthalene dioxygenase (NahC), 2-hydroxy-2*H*-chromene-2-carboxylate isomerase (NahD), *trans-o*-hydroxybenzylidenepyruvic hydratase-aldolase (NahE) and salicylaldehyde dehydrogenase (NahF). The main substrates and products for these enzymes are also depicted. (1) Naphthalene, (2) *cis*-1,2-dihydroxy-1,2-dihydronaphthalene, (3) 1,2-dihydroxynaphthalene, (4) 2-hydroxy-2*H*-chromene-2-carboxylic acid, (5) *trans-o*-hydroxybenzylidenepyruvic acid, (6) salicylaldehyde, (7) pyruvate and (8) salicylic acid (adapted from Peng *et al.*, 2008).

The enzyme NahF (salicylaldehyde dehydrogenase; EC 1.2.1.65; 483 amino acids) catalyzes the last reaction of the upper pathway converting salicylaldehyde to salicylate (Davies & Evans, 1964; Eaton & Chapman, 1992). This enzyme belongs to the aldehyde dehydrogenase (ALDH) superfamily, the members of which oxidize a wide variety of aliphatic and aromatic aldehydes using NAD^+ or $NADP^+$ as a cofactor.

Despite the fact that aldehyde dehydrogenases may share a similar scaffold and modes of oligomerization (dimers or tetramers; Perozich, Nicholas, Lindahl *et al.*, 1999), substrate specificity dictates some of the differences between these enzymes. The salicylaldehyde dehydrogenases, for example, are classified as a family of ALDHs or aromatic ALDHs that oxidize relatively specific aromatic xenobiotics found in the environment (Perozich, Nicholas, Wang *et al.*, 1999). Also belonging to this family are the benzaldehyde dehydrogenase from *P. putida* (Yeung *et al.*, 2008) and vanillin dehydrogenase from *Pseudomonas* sp. strain HR199 (Priefert *et al.*, 1997).

Here, we report the subcloning and expression of recombinant NahF (6×His-NahF) from *P. putida* G7. To elucidate the structural motifs that may distinguish this enzyme from other dehydrogenases, we purified the recombinant protein and aimed to crystallize and collect preliminary diffraction data from 6×His-NahF crystals. As far as we are aware, this is the first crystallization report of an aromatic ALDH.

2. Materials and methods

2.1. Subcloning, protein expression and purification

The NAH7 plasmid from *P. putida* G7 (GenBank nucleotide entry NC_007926.1) was used as the polymerase chain reaction (PCR) template. The primers used to amplify the salicylaldehyde dehydrogenase gene from the NAH7 plasmid were nahF-F, 5′-**CAT ATG** AAG ACA AAA CTG TTT ATC AAC AAC-3′, and nahF-R, 5′-**CTC GAG** TTC AGA AGG GAT ATT GCT GCT-3′. The sites for restriction enzymes (*Nde*I and *Xho*I, respectively) are shown in bold.

The DNA fragments obtained were excised from the gel, purified and ligated into pGEM vector (Promega Corporation). Recombinant plasmid pGEM-*nahF* was used to transform *Escherichia coli* DH5a competent cells. Positive transformants were tested by restriction analysis with *Nde*I and *Xho*I and those presenting the *nahF* gene were propagated and used for construction of the expression vector. DNA fragments obtained from digestion of pGEM-*nahF* with *Nde*I and *Xho*I were ligated into pET28a(TEV) vector (Carneiro *et al.*, 2006) previously digested with the same enzymes. pET28a(TEV) is a modified pET28a vector (Novagen) that adds a 6×His tag followed by a tobacco etch virus (TEV) protease-cleavage site at the N-terminus of the target protein (MGHHHHHHENLYFQGH–target protein). Electrocompetent *E. coli* BL21 Arctic Express (DE3) cells (Agilent Technologies) were transformed by electroporation using a MicroPulser Electroporation Apparatus (Bio-Rad Laboratories) with the recombinant plasmid pET28a(TEV)-*nahF*. Gene insertion was confirmed by colony PCR and sequencing using T7 primers in a MegaBACE instrument (GE Healthcare Life Sciences).

Transformed *E. coli* BL21 Arctic Express (DE3) cells were inoculated in 10 ml LB broth supplemented with 40 µg ml^{-1} gentamicin and 50 µg ml^{-1} kanamycin. Overnight cultures were transferred to 500 ml LB broth without antibiotics and cultivated at 303 K for 3 h. Expression was then induced by addition of IPTG to a final

concentration of 0.5 m*M* and the culture was incubated at 285 K for 24 h at 200 rev min^{-1}.

The bacterial cells were harvested by centrifugation and were resuspended in 20 ml lysis buffer [50 m*M* Tris–HCl pH 7.4, 1%(*w*/*v*) sucrose, 1%(*v*/*v*) Tween 20, 1%(*v*/*v*) glycerol, 0.25%(*w*/*v*) lysozyme]. Cells were ruptured by three cycles of freezing and thawing followed by three cycles of 30 s on/off sonication in an ice–water bath at 30% amplitude. Subsequently, debris was removed by centrifugation at 277 K for 30 min at 10 000*g*.

Imidazole was added to the clear supernatant to a final concentration of 30 m*M* and the solution was immediately loaded onto a 5 ml HisTrap HP affinity column (GE Healthcare Biosciences) pre-equilibrated with five column volumes of equilibration buffer (50 m*M* sodium phosphate buffer pH 7.4, 500 m*M* NaCl, 30 m*M* imidazole) and connected to an ÄKTAprime chromatography system (GE Healthcare Life Sciences). The column was washed at a flow rate of 1.0 ml min^{-1} with five column volumes of equilibration buffer. Subsequently, gradient elution with elution buffer (50 m*M* sodium phosphate buffer pH 7.4, 500 m*M* NaCl, 500 m*M* imidazole) at a flow rate of 5.0 ml min^{-1} was used to elute the retained proteins.

The eluted fractions containing the recombinant NahF (6×His-NahF, 499 amino acids, 54 kDa) from the affinity chromatography were extensively dialyzed against 20 m*M* sodium phosphate buffer pH 7.4 containing 20 m*M* NaCl. Recombinant NahF was further purified on a Superdex 200 gel-filtration column (GE Healthcare) previously equilibrated with 20 m*M* sodium phosphate buffer pH 7.4 with 20 m*M* NaCl and eluted with the same solution (Fig. 2). The peak fractions containing purified 6×His-NahF were analyzed by a dynamic light-scattering (DLS) experiment and the main peak fractions (peak 3, Fig. 2) were pooled and concentrated using a dialysis membrane covered with PEG 8000 powder until a final protein concentration of 15 mg ml^{-1} was achieved. This final 6×His-NahF protein solution was used in crystallization trials.

2.2. Dynamic light-scattering and crystallization assays

The oligomerization state of 6×His-NahF at 2.5 mg ml^{-1} was assessed by a DLS experiment using a DynaPro instrument (Wyatt Technology). The sample tested consisted of elution fractions corresponding to peak 3 from the size-exclusion chromatography (Fig. 2).

Initial crystallization attempts were carried out at 291 K using 24-well plates and the hanging-drop vapour-diffusion method. Drops consisted of 1 µl final 6×His-NahF protein solution and 1 µl of the screening solutions from Crystal Screen and Crystal Screen 2 (Hampton Research) and were equilibrated against 1 ml reservoir solution (screening solution). Initial crystals were only observed in condition No. 5 from Crystal Screen 2, consisting of 2.0 *M* ammonium sulfate and 5%(*v*/*v*) 2-propanol. The condition was optimized by grid screening of the ammonium sulfate concentration and the addition of sodium acetate–acetic acid buffer and *β*-nicotinamide adenine dinucleotide hydrate (NAD$^+$; Sigma–Aldrich) to the crystallization condition. The flower-shaped crystals reached a maximum dimension of 500 µm after 2 d in 2 µl drops equilibrated against 1 ml reservoir solution (Fig. 3).

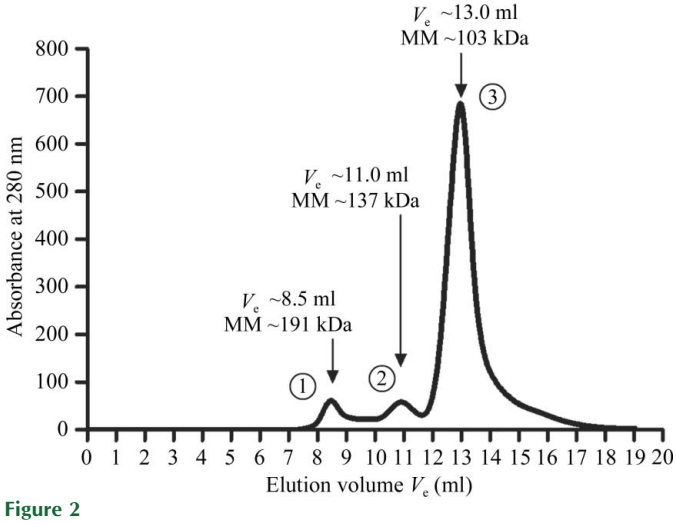

Figure 2
Typical size-exclusion chromatography chromatogram obtained with recombinant NahF. The elution of recombinant NahF in peak 3 (the main peak) corresponds to the profile of a 103 kDa protein and is in good agreement with a dimeric form of 6×His-NahF (108 kDa). The elution volume (V_e) and molecular mass (MM) associated with each peak (1, 2 and 3) are shown.

2.3. Data collection, processing and phase determination

Prior to data acquisition, a flower-shaped 6×His-NahF crystal was carefully broken and a smaller piece (a single 'petal') was harvested using a nylon loop (Hampton Research). The 'petal' was then transferred for a few seconds into a 10 µl drop of a cryogenic solution formed by the addition of 1 µl ethylene glycol to 9 µl reservoir solution. The crystal was then flash-cooled to 100 K in a cold nitrogen stream and used for data acquisition. X-ray diffraction images were recorded on a MAR CCD 165 detector using the D03B-MX1 beamline (Polikarpov *et al.*, 1998) at the Laboratório Nacional de Luz Síncrotron (LNLS), Brazil. Each image was exposed for 60 s with a rotation range of 0.5°.

Diffraction images (Fig. 4) were processed using *iMOSFLM* (Battye *et al.*, 2011) and *SCALA* (Evans, 2006) as distributed in the *CCP*4 package (Winn *et al.*, 1994). Diffraction data statistics are shown in Table 1.

The molecular-replacement (MR) method, as implemented in *Phaser* (McCoy *et al.*, 2007), was used to solve the phase problem with a single monomer of the sheep liver cytosolic aldehyde dehydrogenase crystallographic structure (PDB entry 1bxs; Moore *et al.*, 1998) as the search template. This protein template was chosen as its primary structure shows one of the highest identities (37%) to the NahF amino-acid sequence.

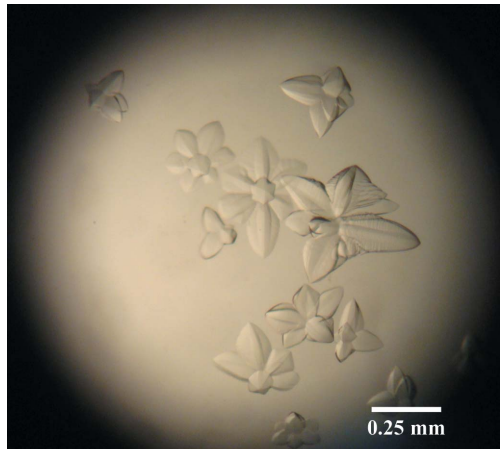

Figure 3
Flower-shaped crystals of recombinant NahF. Crystals were obtained using 1.5 *M* ammonium sulfate, 5%(*v*/*v*) 2-propanol, 5 m*M* NAD$^+$ in 100 m*M* sodium acetate–acetic acid buffer pH 5.0.

Preliminary 6×His-NahF model building was performed using the programs *Buccaneer* (Cowtan, 2006) and *Coot* (Emsley *et al.*, 2010). Restrained refinement of the model was performed by the reciprocal-space refinement program *REFMAC* (Murshudov *et al.*, 2011).

3. Results and discussion

The recombinant salicylaldehyde dehydrogenase from *P. putida* G7 was overexpressed in *E. coli* BL21 Arctic Express cells in a soluble form. Ni^{2+}-affinity and size-exclusion chromatography (SEC) were used to obtain high-purity 6×His-NahF with a yield of approximately 40 mg purified protein per litre of culture. Several attempts to cleave the 6×His tag from the recombinant protein were unsuccessful and subsequent experiments were carried out with 6×His-NahF.

The biological unit of 6×His-NahF appears to be a dimer as suggested by the elution profile in the SEC chromatogram (Fig. 2). This finding is in good agreement with the dynamic light-scattering results, in which the monodisperse sample from SEC peak 3 (with a polydispersity of 14%) exhibits particles with a hydrodynamic radius of 4.7 nm (suggested protein molecular mass of 125 kDa).

Purified 6×His-NahF was concentrated to 15.0 mg ml^{-1} and flower-shaped crystals suitable for diffraction (maximum dimension of 500 µm; Fig. 3) were grown in 1.5 *M* ammonium sulfate, 5%(*v*/*v*) 2-propanol, 5 m*M* NAD^+ in 100 m*M* sodium acetate–acetic acid buffer pH 5.0. Diffraction data collected to 2.42 Å resolution from a broken piece of a flower-shaped crystal indicated that 6×His-NahF crystallized in space group $P6_422$, with unit-cell parameters $a = b = 169.47$, $c = 157.94$ Å (Table 1).

Calculation of the Matthews coefficient suggests the presence of two protein molecules in the asymmetric unit. Surprisingly, all molecular-replacement attempts aiming to find a dimer in the asymmetric unit were unsuccessful. A good MR solution (translation-function *Z* score of 24.7) was only obtained when a monomer was expected in the asymmetric unit ($V_M = 6.06$ Å^3 Da^{-1}; solvent content of almost 80%). This solution and the correct recombinant NahF amino-acid sequence were used as input files in the *Buccaneer* software (Cowtan, 2006) for automated model building. The resulting PDB file was manually adjusted in *Coot* (Emsley *et al.*, 2010) and refined against the original data set in *REFMAC* (Murshudov *et al.*, 1997), achieving *R* and R_{free} values of 25.7% and 28.9%, respectively, prior to the modelling of water molecules.

Inspection of crystal packing shows that a solvent tunnel along the 6_4 screw axis of approximately 90 Å in diameter is responsible for the high solvent content of this crystal. Even though a monomer was observed in the asymmetric unit, the 6×His-NahF biological unit (a dimer) could be generated by a crystallographic twofold axis. The detailed structure of recombinant NahF will be published elsewhere.

Table 1
Summary of diffraction data statistics for the 6×His-NahF crystal.

Values in parentheses are for the lowest/highest resolution shells.

Wavelength (Å)	1.608
Temperature (K)	100
Crystal-to-detector distance (mm)	100
Rotation range per image (°)	0.5
Total rotation range (°)	120
Space group	$P6_422$
Unit-cell parameters (Å)	$a = b = 169.47$, $c = 157.94$
Resolution range (Å)	32.17–2.42 (32.17–7.64/2.55–2.42)
No. of observations	710305 (23697/97367)
No. of unique reflections	51558 (1811/7385)
Data completeness (%)	99.9 (98.7/99.8)
$\langle I/\sigma(I)\rangle$	10.4 (34.8/4.0)
Multiplicity	13.8 (13.1/13.2)
R_{merge}†	0.272 (0.062/0.651)
Average mosaicity (°)	0.38
Wilson *B* factor (Å^2)	18.8
Matthews coefficient (Å^3 Da^{-1})	6.06
Solvent content (%)	79.7

† $R_{merge} = \sum_{hkl}\sum_i |I_i(hkl) - \langle I(hkl)\rangle| / \sum_{hkl}\sum_i I_i(hkl)$, where $I_i(hkl)$ is the *i*th intensity measurement of reflection *hkl* and $\langle I(hkl)\rangle$ is its average.

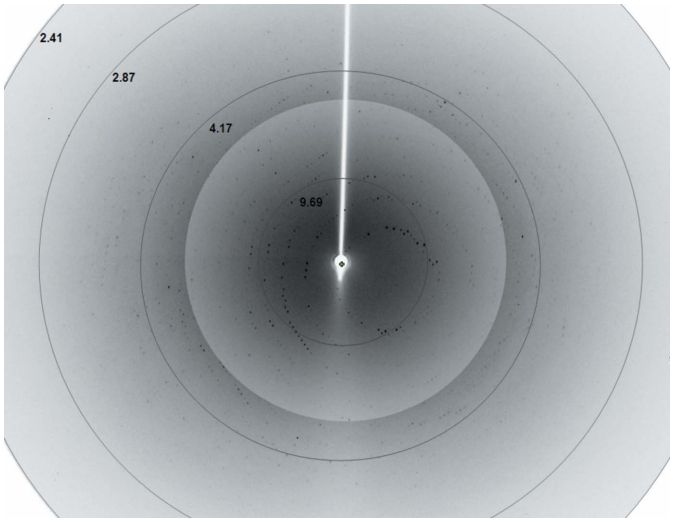

Figure 4
A diffraction image from a broken piece of a flower-shaped 6×His-NahF crystal. Diffraction data were collected to 2.42 Å resolution. The diffraction pattern background around the centre of the image was altered to allow a better visualization of the reflections. Resolution shells are shown (in Å) close to their respective circles.

We would like to thank Dr Masataka Tsuda and Dr Masahiro Sota for kindly providing us with the *P. putida* G7 strain. This work was supported by the Laboratório Nacional de Luz Síncrotron (LNLS; Brazilian Synchrotron Light Laboratory; Project 6970), Conselho Nacional de Desenvolvimento Científico e Tecnológico (CNPq; Project 482173/2010-6) and Fundação de Desenvolvimento à Pesquisa do Estado de Minas Gerais (FAPEMIG; Projects EDT-0185-0.00-07, Rede-170/08 and RDP-00174-10). JBC, DMAC and SLG are recipients of scholarships from Coordenação de Aperfeiçoamento de Pessoal de Nível Superior (CAPES).

References

Annweiler, E., Richnow, H. H., Antranikian, G., Hebenbrock, S., Garms, C., Franke, S., Francke, W. & Michaelis, W. (2000). *Appl. Environ. Microbiol.* **66**, 518–523.
Arun, A., Raja, P. P., Arthi, R., Ananthi, M., Kumar, K. S. & Eyini, M. (2008). *Appl. Biochem. Biotechnol.* **151**, 132–142.
Battye, T. G. G., Kontogiannis, L., Johnson, O., Powell, H. R. & Leslie, A. G. W. (2011). *Acta Cryst.* D**67**, 271–281.
Bosch, R., García-Valdés, E. & Moore, E. R. (1999). *Gene*, **236**, 149–157.
Carneiro, F. R., Silva, T. C., Alves, A. C., Haline-Vaz, T., Gozzo, F. C. & Zanchin, N. I. (2006). *Biochem. Biophys. Res. Commun.* **343**, 260–268.
Cerniglia, C. E. (1984). *Adv. Appl. Microbiol.* **30**, 31–71.
Cowtan, K. (2006). *Acta Cryst.* D**62**, 1002–1011.
Davies, J. I. & Evans, W. C. (1964). *Biochem. J.* **91**, 251–261.
Dennis, J. J. & Zylstra, G. J. (2004). *J. Mol. Biol.* **341**, 753–768.
Eaton, R. W. & Chapman, P. J. (1992). *J. Bacteriol.* **174**, 7542–7554.
Emsley, P., Lohkamp, B., Scott, W. G. & Cowtan, K. (2010). *Acta Cryst.* D**66**, 486–501.
EPA (2004). *Toxicological Review of Naphthalene*. http://oaspub.epa.gov/eims/eimscomm.getfile?p_download_id=501313.
Evans, P. (2006). *Acta Cryst.* D**62**, 72–82.

Habe, H. & Omori, T. (2003). *Biosci. Biotechnol. Biochem.* **67**, 225–243.
Haritash, A. K. & Kaushik, C. P. (2009). *J. Hazard. Mater.* **169**, 1–15.
Holliger, C., Gaspard, S., Glod, G., Heijman, C., Schumacher, W., Schwarzenbach, R. P. & Vazquez, F. (1997). *FEMS Microbiol. Rev.* **20**, 517–523.
IARC (2002). *IARC Monographs on the Evaluation of Carcinogenic Risks to Humans*, Vol. 82. Lyon: IARC.
Kanaly, R. A. & Harayama, S. (2000). *J. Bacteriol.* **182**, 2059–2067.
Li, W., Shi, J., Wang, X., Han, Y., Tong, W., Ma, L., Liu, B. & Cai, B. (2004). *Gene*, **336**, 231–240.
McCoy, A. J., Grosse-Kunstleve, R. W., Adams, P. D., Winn, M. D., Storoni, L. C. & Read, R. J. (2007). *J. Appl. Cryst.* **40**, 658–674.
Moore, S. A., Baker, H. M., Blythe, T. J., Kitson, K. E., Kitson, T. M. & Baker, E. N. (1998). *Structure*, **6**, 1541–1551.
Murshudov, G. N., Skubák, P., Lebedev, A. A., Pannu, N. S., Steiner, R. A., Nicholls, R. A., Winn, M. D., Long, F. & Vagin, A. A. (2011). *Acta Cryst.* D**67**, 355–367.
Park, S.-Y., Lee, S.-M., Ye, S.-K., Yoon, S.-H., Chung, M.-H. & Choi, J. (2006). *Toxicol. Lett.* **167**, 27–33.
Peng, R.-H., Xiong, A.-S., Xue, Y., Fu, X.-Y., Gao, F., Zhao, W., Tian, Y.-S. & Yao, Q.-H. (2008). *FEMS Microbiol. Rev.* **32**, 927–955.
Perozich, J., Nicholas, H., Lindahl, R. & Hempel, J. (1999). *Adv. Exp. Med. Biol.* **463**, 1–7.
Perozich, J., Nicholas, H., Wang, B.-C., Lindahl, R. & Hempel, J. (1999). *Protein Sci.* **8**, 137–146.
Polikarpov, I., Perles, L. A., de Oliveira, R. T., Oliva, G., Castellano, E. E., Garratt, R. C. & Craievich, A. (1998). *J. Synchrotron Rad.* **5**, 72–76.
Priefert, H., Rabenhorst, J. & Steinbüchel, A. (1997). *J. Bacteriol.* **179**, 2595–2607.
Rosselló-Mora, R. A., Lalucat, J. & García-Valdés, E. (1994). *Appl. Environ. Microbiol.* **60**, 966–972.
Saeed, M., Higginbotham, S., Gaikwad, N., Chakravarti, D., Rogan, E. & Cavalieri, E. (2009). *Free Radic. Biol. Med.* **47**, 1075–1081.
Samanta, S. K., Singh, O. V. & Jain, R. K. (2002). *Trends Biotechnol.* **20**, 243–248.
Spink, D. C., Wu, S. J., Spink, B. C., Hussain, M. M., Vakharia, D. D., Pentecost, B. T. & Kaminsky, L. S. (2008). *Toxicol. Appl. Pharmacol.* **226**, 213–224.
Stohs, S. J., Ohia, S. & Bagchi, D. (2002). *Toxicology*, **180**, 97–105.
Topinka, J., Marvanová, S., Vondrácek, J., Sevastyanova, O., Nováková, Z., Krcmár, P., Pencíková, K. & Machala, M. (2008). *Mutat. Res.* **638**, 122–132.
Winn, M. D. *et al.* (2011). *Acta Cryst.* D**67**, 235–242.
Yang, Y., Chen, R. F. & Shiaris, M. P. (1994). *J. Bacteriol.* **176**, 2158–2164.
Yen, K.-M. & Gunsalus, I. C. (1982). *Proc. Natl Acad. Sci. USA*, **79**, 874–878.
Yen, K.-M. & Gunsalus, I. C. (1985). *J. Bacteriol.* **162**, 1008–1013.
Yeung, C. K., Yep, A., Kenyon, G. L. & McLeish, M. J. (2008). *Biochim. Biophys. Acta*, **1784**, 1248–1255.